# A Detailed Examination of Gas and Liquid Phase Transient Processes in Convective Droplet Evaporation

**R. J. Haywood**
Graduate Student.

**R. Nafziger**
Graduate Student.

**M. Renksizbulut**
Associate Professor.

University of Waterloo,
Mechanical Engineering Department,
Waterloo, Ontario, Canada N2L 3G1

*A finite volume numerical technique has been used to model the evaporation of an n-heptane droplet with an initial Reynolds number of 100 in air at 800 K, 1 atm. The effects of variable thermophysical properties, liquid phase motion and heating, and transient variations in droplet size and velocity are included in the analysis. With appropriate corrections for the effects of variable properties and liquid phase heating, quasi-steady correlations are shown to predict accurately the transient histories of the drag coefficient and Nusselt and Sherwood numbers. For the case investigated here, the transient effects of importance were the variation in droplet velocity, the decline in the liquid phase velocities, and the rise in the droplet surface and volume average temperatures. In spite of the transient rise in the droplet temperature, the nature of the liquid phase heating, as characterised by the liquid Nusselt number, was found to remain constant during most of the droplet lifetime.*

## 1 Introduction

Evaporation of droplets in high-temperature convective environments is of substantial importance in a large number of practical industrial processes. Typical combustion chamber conditions and fuel spray patternation in diesel and rocket engines and gas turbines make convective evaporation at intermediate Reynolds number ($\mathrm{Re} = O(100)$) the predominant mode of droplet vaporization. Despite many years of research, further understanding of isolated droplet evaporation in the intermediate Reynolds number regime, including the effects of all gas and liquid phase transients, variable thermophysical properties, and liquid phase heat and momentum transport, is still required. In particular, the literature demonstrates a lack of consensus as to the transport processes that may be considered quasi-steady. Although most researchers acknowledge the large temperature differences intrinsic to the physical problem, few have attempted to include property variations in their models. Finally, the exact nature of liquid phase momentum and heat transfer processes for a realistic droplet are not well characterized without simplifying assumptions in either the continuous or dispersed phases. Because this work is concerned with evaporation in the intermediate Reynolds number regime, the large volume of literature dealing with droplet evaporation and combustion at very low and zero Reynolds numbers will not be discussed in the following literature review.

Using a boundary layer analysis, Prakash and Sirignano (1980) examined the convective evaporation of *n*-hexane, *n*-decane, and *n*-hexadecane droplets at 10 atm ambient pressure. Based on the observation that the gas phase residence time $2R^*/U^*_\infty$ is typically much shorter than the droplet lifetime, quasi-steadiness was assumed in all gas phase transport processes. Similarly, because the characteristic time required to establish steady liquid phase motion is much smaller than the droplet lifetime, liquid motion was assumed to behave in a quasi-steady manner. Despite finding liquid phase heating a source of unsteadiness persisting throughout most of the droplet lifetime, the quasi-steady correlations of Ranz and Marshall (1952) and Spalding (1953) were found to agree well with the results, provided an appropriate correction was made for the effects of the unsteady liquid phase heat flux. Summarizing the results of their approximate analytical solutions in a review article, Sirignano (1983) concluded that because transient heating of the droplet surface continues throughout the droplet lifetime without the surface reaching the boiling point temperature, no justification can be found for a quasi-steady assumption with respect to liquid phase heating.

Sundararajan and Ayyaswamy (1984), following similar characteristic time arguments, studied condensation on droplets at intermediate Reynolds numbers, assuming quasi-steady behavior in all processes but liquid phase heating. Because of the differences between the evaporation and condensation processes, their observations cannot readily be applied to droplet evaporation. Furthermore, because their analysis, as well as that of Prakash and Sirignano (1980), allows transient behavior only in the liquid phase heating, the importance of transient effects in the gas and liquid phases, the motion of the receding gas/liquid interface, and global transients such as droplet deceleration, are still inadequately addressed.

Dwyer and Sanders (1984a, 1984b) modeled the convective evaporation of dodecane droplets at ambient pressures of 1, 5, and 25 atm. A sophisticated numerical technique, using an adaptive grid to track the shrinking droplet, was employed. The model included the effects of transients in both phases as well as the transient deceleration of the droplet under the influence of its own drag. Variations in surface mass transfer due to droplet heating were found to be the primary cause of unsteadiness. Because drag coefficients and Nusselt numbers were found to have values lower than quasi-steady correlations would predict, it was concluded that there were large deviations from quasi-steady behavior in heat, mass, and momentum transport during the droplet lifetime. Particularly puzzling are their predictions of the drag coefficient, which not only show a decreasing trend with decreasing Reynolds number, but also indicate a very large reduction in drag due to vaporization. These trends contradict well known experimental observations (e.g., see Yuen and Chen, 1976).

In direct contrast to these conclusions, numerical studies by Renksizbulut and Haywood (1986, 1988) showed that the instantaneous drag coefficients and Nusselt numbers of droplets of *n*-heptane evaporating in their own vapor at 1 and 10 atm could be predicted using the correlations of Renksizbulut and Yuen (1983, 1983b) provided that a suitable correction is made for the effects of liquid phase heating. Further, it was demonstrated that complete droplet life histories could be

Contributed by the Heat Transfer Division for publication in the JOURNAL OF HEAT TRANSFER. Manuscript received by the Heat Transfer Division March 22, 1988. Keywords: Evaporation, Sprays/Droplets, Transient and Unsteady Heat Transfer.

predicted using a simple analytical model that utilized correlations in a quasi-steady manner together with an enhanced diffusion model for liquid heating. The liquid heating model accounted for the effects of liquid motion through the use of an effective thermal conductivity. The predictive abilities of the simple analytical model were better at lower ambient pressures. It was concluded that unsteady gas phase effects, resulting from perturbations to the velocity and temperature fields due to the higher surface regression rate at higher pressures, were responsible for the departure from quasi-steady behavior. The effects of increased surface motion and second-order drag effects, which are more pronounced at elevated pressures (Faeth, 1983), may have contributed to the observed departure because the correlations used in the model do not acknowledge these effects.

From the previous discussion it becomes clear that many of the important phenomena associated with convective droplet evaporation occur within the liquid phase. In order to assess the impact of liquid heating on droplet combustion, Law (1976) and Law and Sirignano (1977) examined the two limiting cases of; (*i*) rapid mixing in which the liquid thermal conductivity is assumed to be infinite due to the presumed intense liquid phase motion, and (*ii*) the conduction limit corresponding to a motionless liquid phase. Although useful in defining the envelope of possible liquid phase behaviors, the physical reality does not approach either of these limits. Detailed numerical results of Renksizbulut and Haywood (1986, 1988) show an initial period of rapid mixing and corresponding high rates of liquid heating associated with the establishment of a toroidal temperature field followed by a more gradual heating as the diffusion of heat proceeds normal to the established pattern of closed isotherms.

In order to understand more completely the liquid phase processes, many researchers have decoupled the problem and, while making simplifying assumptions with respect to the behavior of the continuous phase, have solved the heat, mass, and momentum transport phenomena within the liquid phase alone. Johns and Beckmann (1966) studied numerically the liquid phase mass transport, subject to the assumptions of a creeping flow velocity field in the liquid phase (the Hadamard–Rybczynski solution), and negligible continuous phase resistance to mass transfer. The observed transient liquid Nusselt number behavior consisted of a rapid initial decline followed by an oscillatory approach to an asymptotic value. For liquid Peclet numbers in excess of 60 the asymptotic Nusselt number was within 5 percent of the Kronig and Brink (1950) limit of 17.9 attained at infinite Peclet number. In terms of a general qualitative understanding of liquid phase transport phenomena, this analysis provides insight, but neglecting the transient effects of droplet deceleration and evaporation, as well as imposing a liquid phase velocity field valid only in creeping flow, limit its application in realistic cases.

Assuming an approximate surface shear stress distribution due to the relative motion of the gas with respect to the droplet, Prakash and Sirignano (1978) studied liquid droplet heating with internal circulation. The liquid motion was taken to be quasi-steady and to consist of a thin laminar boundary layer at the gas/liquid interface and an inviscid core behaving as a Hills spherical vortex. This liquid phase model was later coupled to a gas phase analysis as discussed previously. Liquid phase motion was found to reduce the time required to establish nearly uniform temperature profiles in the droplet but not toward the (instantaneous) limit suggested by a rapid mixing model. While this analysis includes many of the important gas phase phenomena that influence liquid phase motion and heating, several weaknesses still exist. The transient reduction in droplet Reynolds number and the associated reduction in liquid Peclet number may alter the nature of liquid heating during the droplet lifetime. The boundary layer analysis also neglects the wake region, making it impossible to determine the drag coefficient. Furthermore the contribution to heat and mass transfer from this region is not entirely negligible.

In this paper the evaporation of an isolated *n*-heptane

## Nomenclature

$B_H$ = heat transfer number $= c^*_{P,g}(T^*_\infty - T^*_s)/L^*_s$
$B_M$ = mass transfer number $= (Y_{F,s} - Y_{F,\infty})/(1 - Y_{F,s})$
$c_P$ = specific heat at constant pressure $= c^*_P/c^*_{P,\infty}$
$C_D$ = total drag coefficient $= C_F + C_P + C_T$
$C_F$ = friction drag coefficient $= 2F^*_F/(\rho^*_\infty v^{*2}_\infty \pi R^{*2})$
$C_P$ = pressure drag coefficient $= 2F^*_P/(\rho^*_\infty v^{*2}_\infty \pi R^{*2})$
$C_T$ = thrust coefficient $= 2F^*_T/(\rho^*_\infty v^{*2}_\infty \pi R^{*2})$
$\mathfrak{D}$ = species diffusion coefficient $= \mathfrak{D}^*/\mathfrak{D}^*_\infty$
$F^*$ = force
$h^*_H$ = heat transfer coefficient
$h^*_M$ = mass transfer coefficient
$k$ = thermal conductivity $= k^*/k^*_\infty$
$L_s$ = latent heat of vaporization $= L^*_s/(c^*_{P,\infty} T^*_\infty)$
$\dot{m}^*$ = total evaporation rate
$\dot{m}''_\theta$ = local mass flux $= \dot{m}''^*_\theta/(\rho^*_\infty v^*_{\infty,o})$
$M$ = molecular weight
Nu = Nusselt number $= 2R^* h^*_H/k^*$
$p$ = pressure $= (p^* - p^*_\infty)/(\rho^*_\infty v^{*2}_{\infty,o})$
Pr = Prandtl number $= \mu^* c^*_P/k^*$
$Q^*$ = heat transfer rate
$r$ = radial coordinate $= r^*/R^*$
$R$ = instantaneous drop radius $= R^*/R^*_o$
$\mathfrak{R}$ = universal gas constant
Re = Reynolds number $= 2R^* \rho^* v^*_\infty/\mu^*$
$\mathrm{Re}_m$ = Reynolds number $= 2R^* \rho^*_\infty v^*_\infty/\mu^*_f$
Sh = Sherwood number $= 2R^* h^*_M/(\rho^* \mathfrak{D}^*)$
Sc = Schmidt number $= \mu^*/(\rho^* \mathfrak{D}^*)$
$t$ = time $= t^* v^*_{\infty,o}/R^*_o$
$T$ = temperature $= T^*/T^*_\infty$
$v^*_\infty$ = instantaneous free-stream velocity
$V$ = instantaneous free-stream velocity $= v^*_\infty/v^*_{\infty,o}$
$v_r$ = radial velocity component $= v^*_r/v^*_\infty$
$v_\theta$ = tangential velocity component $= v^*_\theta/v^*_\infty$
$X$ = mole fraction
$Y$ = mass fraction
$\theta$ = tangential coordinate
$\mu$ = viscosity $= \mu^*/\mu^*_\infty$
$\rho$ = density $= \rho^*/\rho^*_\infty$
$\tau_{r\theta}$ = shear stress $= \tau^*_{r\theta}/(\mu^*_\infty v^*_\infty/R^*)$
$\tau_{rr}$ = normal shear $= \tau^*_{rr}/(\mu^*_\infty v^*_\infty/R^*)$
$\phi$ = generalized variable

### Subscripts and Superscripts

$A$ = air component
$f$ = film conditions
$F$ = fuel component
$g$ = gas phase
$H$ = heat transfer
$l$ = liquid phase
$M$ = mass transfer
$o$ = initial conditions
$r$ = thermal radiation
$s$ = at the droplet surface
$\theta$ = local
$\infty$ = free-stream conditions
$^*$ = dimensional quantity
$\hat{}$ = unit vector
$\tilde{}$ = tensor
$\bar{}$ = spatial average

**Table 1 Nondimensional governing equations**

THE GOVERNING EQUATIONS

$$\frac{\partial}{\partial t}(\rho V R\phi) + V^2\vec{\nabla}\cdot\left\{\rho\phi\left[\left(v_r - \frac{r}{V}\frac{dR}{dt}\right)\hat{r} + v_\theta\hat{\theta}\right]\right\} = \frac{V}{R}\vec{\nabla}\cdot\left(\Gamma_\phi\vec{\nabla}\phi\right) + S_\phi \quad (1)$$

| Equation | $\phi$ | $\Gamma_\phi$ | $S_\phi$ |
|---|---|---|---|
| Continuity | 1 | 0 | $S_C$ |
| Radial Momentum | $v_r$ | $2\mu/Re_{\infty,o}$ | $S_{RM}$ |
| Tangential Momentum | $v_\theta$ | $2\mu/Re_{\infty,o}$ | $S_{TM}$ |
| Energy | $T$ | $2k/(c_P Re_{\infty,o}Pr_\infty)$ | $S_E$ |
| Species | $Y_F$ | $2\rho\mathcal{D}/(Re_{\infty,o}Sc_\infty)$ | $S_Y$ |

where:

$$S_C = \rho R\frac{dR}{dt} - 2\rho V\frac{dR}{dt}$$

$$S_{RM} = V^2\left[\vec{\nabla}\cdot(\rho\vec{v}v_r) - \vec{\nabla}\cdot(\rho\vec{v}\vec{v})_r\right] - \frac{2V}{\mathrm{Re}_{\infty,o}R}\left[\vec{\nabla}\cdot\mu\vec{\nabla}v_r - \left(\vec{\nabla}\cdot\tilde{\tau}\right)_r\right] - 2\rho V v_r\frac{dR}{dt} - \frac{\partial p}{\partial r} - \rho R\cos\theta\frac{dV}{dt}$$

$$S_{TM} = V^2\left[\vec{\nabla}\cdot(\rho\vec{v}v_\theta) - \vec{\nabla}\cdot(\rho\vec{v}\vec{v})_\theta\right] - \frac{2V}{\mathrm{Re}_{\infty,o}R}\left[\vec{\nabla}\cdot\mu\vec{\nabla}v_\theta - \left(\vec{\nabla}\cdot\tilde{\tau}\right)_\theta\right] - 2\rho V v_\theta\frac{dR}{dt} - \frac{1}{r}\frac{\partial p}{\partial\theta} + \rho R\sin\theta\frac{dV}{dt}$$

$$S_E = \rho TR\frac{dV}{dt} - 2\rho TV\frac{dR}{dt} + \frac{2V}{\mathrm{Re}_{\infty,o}\mathrm{Pr}_\infty R}\frac{k}{c_P^2}\left(\vec{\nabla}T\cdot\vec{\nabla}c_P\right) + \frac{2V}{\mathrm{Re}_{\infty,o}\mathrm{Sc}_\infty R}\left(\frac{c_{P,F}-c_{P,A}}{c_P}\right)\rho\mathcal{D}\left(\vec{\nabla}T\cdot\vec{\nabla}Y_F\right)$$

$$S_Y = \rho Y_F R\frac{dV}{dt} - 2\rho Y_F V\frac{dR}{dt}$$

droplet with an initial Reynolds number of 100 at an ambient 800 K and 1 atm is examined. A numerical finite volume analysis is employed and all transients and variable property effects are included in both gas and liquid phases. An assessment will be made of the importance of all transient processes in gas and liquid phases including the shrinkage of the liquid droplet and the resulting motion of the gas/liquid interface, the deceleration of the droplet under the influence of its own drag and its effect on liquid phase motion, and the transient heating of the droplet interior. The ability of quasi-steady correlations in prediction of instantaneous drag coefficients and Nusselt and Sherwood numbers will be examined. The detailed nature of transport phenomena at the gas liquid interface as well as the liquid phase motion and heating will be presented and discussed. It is hoped that the detailed information presented in this paper will serve as benchmark data against which future analytical and numerical models may be compared.

## 2 Mathematical and Numerical Model

In the formulation of the problem it has been assumed that: (*i*) The droplet maintains a spherical shape, (*ii*) the flow field is laminar and axisymmetric, (*iii*) there are no external body forces, (*iv*) thermal radiative, viscous dissipation, Soret and Dufour effects and pressure diffusion are negligible, (*v*) thermodynamic equilibrium prevails at the gas/liquid interface, and (*vi*) air is insoluble in the liquid droplet. All effects due to variable thermophysical properties, liquid phase motion and heating, and transient variations in droplet size and velocity are included in the analysis. Expressions for conservation of mass, momentum, energy, and species in spherical polar coordinates, subject to the above assumptions, and nondimensionalized as outlined in the nomenclature section, are given in Table 1.

Nondimensionalizing lengths and velocities according to instantaneous values is done for convenience in the numerical modeling. In the transformed coordinates the boundary far from the droplet and the gas/liquid interface remain stationary and boundary conditions far from the droplet remain temporally constant. The penalty paid for this convenience is manifested in the extra terms appearing in the governing equations. The boundary conditions are given in Table 2.

**Table 2 Nondimensionalized boundary conditions; for the present study $r_\infty = 40$**

BOUNDARY CONDITIONS

| | | |
|---|---|---|
| Gas/liquid interface: | $T_{\ell,s} = T_{g,s}$ , | $v_{\theta,\ell,s} = v_{\theta,g,s}$ |
| $(r = 1, 0 \le \theta \le \pi)$ | $-\left(k\frac{\partial T}{\partial r}\right)_{\ell,s} = -\left(k\frac{\partial T}{\partial r}\right)_{g,s} + \frac{1}{2}\mathrm{Re}_{\infty,o}\mathrm{Pr}_\infty R\dot{m}''_\theta L_s$ | |
| | $\dot{m}''_\theta = \frac{2}{\mathrm{Re}_{\infty,o}\mathrm{Sc}_\infty}\left[\frac{-\rho\mathcal{D}}{R(1-Y_F)}\frac{\partial Y_F}{\partial r}\right]_{g,s}$ | |
| | $X_{F,s} = p^*_{F,s}\left(T^*_s\right)/p^*_\infty$ | |
| | $v_{r,\ell,s} = \frac{1}{V}\left(\frac{\dot{m}''_\theta}{\rho_{\ell,s}} + \frac{dR}{dt}\right)$ ; | $v_{r,g,s} = \frac{1}{V}\left(\frac{\dot{m}''_\theta}{\rho_{g,s}} + \frac{dR}{dt}\right)$ |
| | $\mu_{\ell,s}\left(\frac{\partial v_\theta}{\partial r} - \frac{v_\theta}{r} + \frac{1}{r}\frac{\partial v_r}{\partial\theta}\right)_{\ell,s}$ | $= \mu_{g,s}\left(\frac{\partial v_\theta}{\partial r} - \frac{v_\theta}{r} + \frac{1}{r}\frac{\partial v_r}{\partial\theta}\right)_{g,s}$ |
| Free stream inlet: | $T = 1$ | $Y_F = 0$ |
| $(r = r_\infty, 0 \le \theta \le \pi/2)$ | $v_r = -\cos\theta$ | $v_\theta = \sin\theta$ |
| Free stream outlet: | $\frac{\partial\phi}{\partial r} = 0$ ; | $\phi = v_r, v_\theta, T, Y_F$ |
| $(r = r_\infty, \pi/2 \le \theta \le \pi)$ | | |
| Axes of symmetry: | $\frac{\partial\phi}{\partial\theta} = 0$ ; | $\phi = v_r, T, Y_F$ |
| $(0 \le r \le r_\infty, \theta = 0, \pi)$ | $v_\theta = 0$ | |
| Origin: | $\frac{\partial\phi}{\partial r}\Big)_{\theta=\pi/2} = 0$ ; | $\phi = v_r, T, Y_F$ |
| $(r = 0)$ | | |

Expressions for overall conservation of mass and momentum complete the mathematical model and are as follows:

*Conservation of Mass:*

$$\frac{dR}{dt} = -\frac{1}{2\bar{\rho}_l}\left(\int_0^\pi \dot{m}''_\theta\sin\theta\, d\theta + \frac{2}{3}R\frac{d\bar{\rho}_l}{dt}\right) \quad (2)$$

*Conservation of Momentum:*

$$\frac{dV}{dt} = -\frac{3}{8}\frac{C_D V^2}{\bar{\rho}_l R} \quad (3)$$

For completeness the definitions of drag coefficients, Nusselt, and Sherwood numbers are also given here

$$C_F = \frac{8}{\mathrm{Re}_{\infty,o}RV}\int_0^\pi (\tau_{r\theta}\sin\theta - \tau_{rr}\cos\theta)_s\sin\theta\, d\theta \quad (4)$$

$$C_P = \frac{4}{V^2}\int_0^\pi p_s\cos\theta\sin\theta\, d\theta \quad (5)$$

$$C_T = 2\int_0^\pi \rho_g\left(v_r^2\sin 2\theta - 2v_r v_\theta\sin^2\theta\right)_s d\theta \quad (6)$$

$$\mathrm{Nu}_\infty = \frac{1}{2}\int_0^\pi \left(\frac{2k_g}{1-T}\frac{\partial T}{\partial r}\right)_{s,\theta}\sin\theta\, d\theta \quad (7)$$

$$\mathrm{Sh}_\infty = \frac{1}{2}\int_0^\pi \left(\frac{2\rho_g\mathcal{D}}{Y_{F,\infty}-Y_F}\frac{\partial Y_F}{\partial r}\right)_{s,\theta}\sin\theta\, d\theta \quad (8)$$

Clearly the coupled, nonlinear transport equations and boundary conditions forming the mathematical model do not admit an exact analytical solution and for this reason a numerical approach was taken. Integration of the transport equations over discrete control volumes and discrete time steps led to the formation of sets of linearized equations of the form:

$$a_P\phi_P = a_N\phi_N + a_S\phi_S + a_E\phi_E + a_W\phi_W + b \quad (9)$$

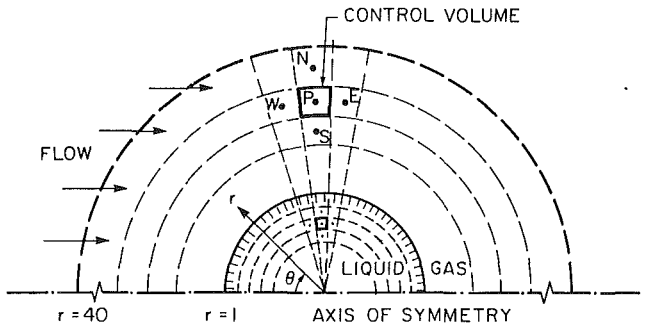


**Fig. 1 The numerical solution domain and grid layout**

relating the value of $\phi$ at any point $P$ to the values at the neighboring points $N$, $S$, $E$, and $W$, as shown in Fig. 1. The linearized equation sets were solved using an iterative line Gauss-Seidel method with overrelaxation. Iteration at the coefficient level is also necessary due to the nonlinearity of the coefficients $a_{N,S,E,W,P}$ and $b$. Boundary conditions at the gas/liquid interface were implemented by discretizing the governing boundary conditions for special interface control volumes of zero thickness, leading to equations similar in form to equation (9). In this way, simultaneous solution of both phases could be accomplished, ensuring a direct and accurate coupling. Details of the lengthy derivation leading to equation (9), the thermophysical properties used, and other aspects of the numerical procedure are given in the theses by Haywood (1986) and Nafziger (1988).

The numerical grid, shown in Fig. 1, was formed of orthogonal annular control volumes bounded by lines of constant $r$ and $\theta$, with 45 control volumes tangentially equally spaced at 4 deg intervals and 70 control volumes radially unequally spaced. On the liquid side 20 radial control volumes with a nondimensional spacing of $\Delta r = 0.0125$ adjacent to the droplet surface flaring at a rate of 12.9 percent toward the origin were used. In the gas phase 50 radial control volumes with $\Delta r = 0.0125$ at the droplet surface and flaring at a rate of 12.7 percent were employed resulting in $r_\infty = 40$.

Because there are no known exact solutions for the problem under investigation, it was necessary to test the accuracy of the numerical predictions by comparison to existing benchmark experimental and numerical correlations for test problems that isolated relevant aspects of the complete problem. Predicted total drag values for isothermal solid spheres at Reynolds numbers between 1 and 250 were within 1 percent of the experimental correlation of Clift et al. (1978). The point of flow separation was predicted within 0.5 deg and the trailing vortex length within 3 percent of experimentally observed values. Predicted component drag values were within 1 percent of the numerical predictions of Cliffe and Lever (1984) and total drag values for isothermal liquid spheres at Reynolds numbers between 100 and 300 were within 1 percent of the numerical data of LeClair and Hamilec (1972). Total drag coefficients and Nusselt numbers agreed within 1 and 2 percent, respectively, of the correlations of Renksizbulut and Yuen (1983a, 1983b) for solid spheres with heat transfer.

Because economic constraints preclude extensive grid refinement studies for the complete transient problem, the study of solution sensitivity to the size and shape of the grid were restricted to the test problems previously mentioned. Tangential control volume spacings of 3, 4, and 5 deg, corresponding to 60, 45, and 30 tangential control volumes, respectively, affected drag values by less than 1 percent. The use of 30 rather than 20 control volumes radially in the liquid phase resulted in less than 0.1 percent change in the gas/liquid interface velocity and negligible change in the liquid vortex center location. The use of up to 80 radial control volumes in the gas phase, covering a range of $r_\infty$ between 20 and 80, with

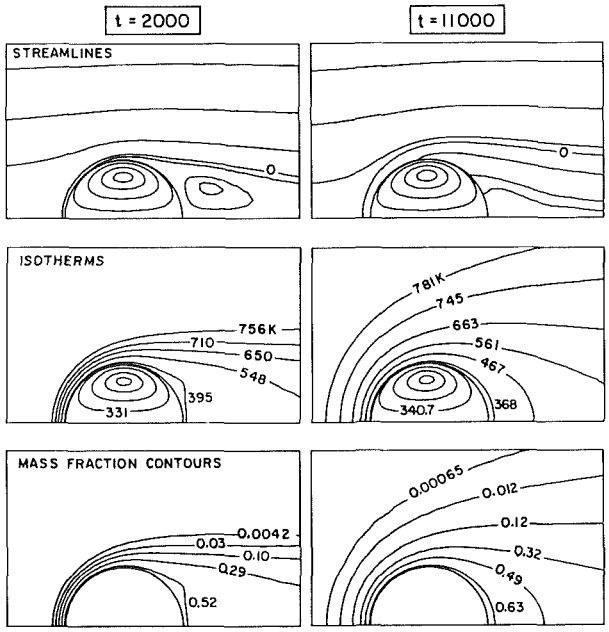


**Fig. 2 Streamlines, isothermals, and mass fraction contours at $t = 2000$ and 11,000. The remaining liquid phase isothermals are 323 K, 315 K, 312 K at $t = 2000$, and 340.5 K, 340.4 K, 340.3 K at $t = 11{,}000$.**

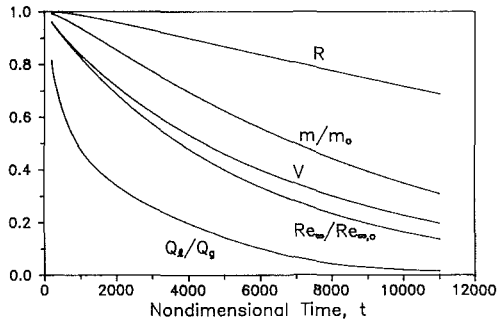


**Fig. 3 Droplet radius, mass, velocity, Reynolds number, and liquid heating fraction histories**

either a smaller rate of grid flare or smaller control volumes, resulted in changes of predicted drag values of less than 1 percent. The timestep sensitivity of the numerical solution was investigated through a series of trials of timestep-halving at various times throughout the transient development. For example, a test involving 100 timesteps corresponding to about 5 percent of the total droplet lifetime resulted in accumulated differences less than 0.2 percent in the key parameters of interest such as $R$, $V$, $C_D$, Nu, and Sh. Hence the results are believed to be reasonably grid and timestep independent.

## 3 Results and Discussion

The following results describe the life history of an $n$-heptane droplet evaporating in air at 800 K and 1 atm pressure. The droplet is initially uniform in temperature at 298 K with no internal motion and has an initial Reynolds number of 100 based on free-stream thermophysical properties.

Streamlines, isotherms, and isomass contour plots are shown in Fig. 2 at two times during the droplet lifetime. Qualitatively, the importance of convection in both the liquid and gas phases is apparent: in the gas phase by the fore-aft nonsymmetry; and in the liquid phase by the similarity between the streamlines and isotherms. The effect of surface blowing due to vaporization is also noted in the displacement of the zero streamline away from the droplet surface. The

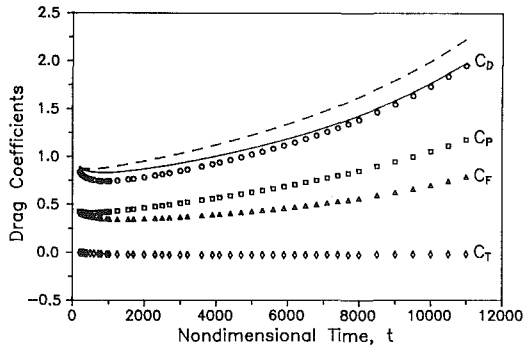


**Fig. 4 Drag coefficients; ○—fully numerical solution;—equation (10); - - - Yuen and Chen (1976) correlation; □—$C_P$; Δ—$C_F$; ◇—$C_T$**

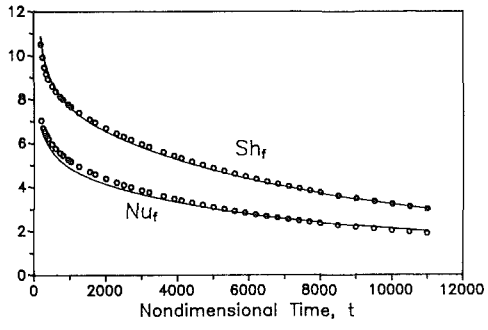


**Fig. 5 Nusselt and Sherwood number histories; ○—fully numerical solution;—equation (12) for Nu and equation (13) for Sh**

transient Reynolds number, liquid heating fraction, velocity, radius, and mass histories are shown in Fig. 3. The droplet spends a significant portion of its lifetime at Reynolds numbers where convection effects are dominant, although it is arguable whether the assumption of boundary layer behavior is valid especially at later times. Liquid heating persists for about the first half of the droplet lifetime in the present case. With higher vaporization rates expected at elevated pressures, liquid heating will persist for a greater portion of the lifetime. Because the time required to heat the droplet is of the same order as the droplet lifetime, liquid heating is an important source of unsteady behavior.

Figures 4 and 5 show the transient histories of the momentum, heat, and mass transfer rates as characterized by the total drag coefficient, Nusselt, and Sherwood numbers, respectively. Except for an early rapid reduction, the total drag coefficient follows the expected increasing trend as the droplet Reynolds number decreases. The early reduction in $C_D$ is caused by the modification of the flow field and transport properties in the vicinity of droplet surface with the onset of evaporation. Specifically, vaporization acts to decrease drag by (*i*) thickening the boundary layer and thus reducing the shear stress at the droplet surface, and (*ii*) reducing the mixture viscosity in the gas phase boundary layer by increasing the concentration of cold fuel vapor. Following the methodology of Haywood and Renksizbulut (1986) the drag history can be predicted based on the drag correlation of Renksizbulut and Yuen (1983a)

$$C_D(1+B'_{Hf})^{0.2} = \frac{24}{\mathrm{Re}_m}(1+0.2\mathrm{Re}_m^{0.63}); \quad 10 \le \mathrm{Re}_m \le 300 \tag{10}$$

where

$$B'_{Hf} = \frac{c^*_{Pf}(T^*_\infty - \bar{T}^*_s)}{L^*_s}\left(1 - \frac{Q_l}{Q_g} + \frac{Q_r}{Q_g}\right) \tag{11}$$

The quasi-steady prediction of this correlation is in good agreement with the numerical data as seen in Fig. 4. Some departure is observed earlier in the droplet lifetime when the droplet surface mobility is strongest. This is consistent with the fact that the right-hand side of equation (10) is based on the standard drag curve for solid spheres. Although some attempts have been made (Nafziger, 1988) to modify equation (10) for the effects of surface mobility, there are insufficient data at the present time to achieve this objective.

Figure 4 also shows the component drag histories. Pressure drag is found to be the dominant drag component throughout the droplet lifetime. This is consistent with the fact that blowing due to evaporation reduces friction drag but at the same time destabilizes the boundary layer leading to early flow separation and hence higher pressure drag as compared to the solid sphere case. Thrust caused by asymmetric surface mass efflux was found to be negligible, contributing to at most 3 percent reduction in $C_D$. Surprisingly the major contribution to $C_T$ comes from the second term of the integral in equation (6). Yuen and Chen (1976) have proposed using the standard drag curve with the viscosity in the Reynolds number based on the one-third reference state. As shown in Fig. 4 this approach did not produce encouraging results.

The transient heat transfer behavior in some respects parallels that of the momentum transfer. With the onset of surface blowing, the thickening boundary layer and reduced thermal conductivity in the cold, fuel-rich region near the droplet surface both act to impede the transfer of energy to the droplet surface, and a rapid initial decline in the Nusselt number is observed. Once blowing is established the slowly decreasing Reynolds number and associated reduced convective transport lead to a more gentle decreasing trend in Nu. Again, with appropriate modification for the effects of liquid phase heating, variable properties, and surface blowing, the Nusselt number history is predicted reasonably well by the Renksizbulut-Yuen (1983b) correlation

$$\mathrm{Nu}_f(1+B'_{Hf})^{0.7} = 2 + 0.57\mathrm{Re}_m^{1/2}\mathrm{Pr}_f^{1/3}; \quad 20 \le \mathrm{Re}_m \le 2000 \tag{12}$$

As expected, the transient dynamics of the mass transfer are very similar to the heat transfer. The thickened boundary layer and modified properties in the cold, fuel-rich boundary rapidly decrease the mass transfer during the initial stages of evaporation. A more gentle decrease in the Sherwood number is then observed, owing to the reduced convection effects as the Reynolds number decays. The following quasi-steady mass transfer correlation, similar in form to the Nusselt number correlation, predicts the transient Sherwood number behavior with good accuracy:

$$\mathrm{Sh}_f(1+B_M)^{0.7} = 2 + 0.87\mathrm{Re}_m^{1/2}\mathrm{Sc}_f^{1/3}; \quad 20 \le \mathrm{Re}_m \le 2000 \tag{13}$$

where

$$B_M = \frac{\bar{Y}_{F,s} - Y_{F,\infty}}{1 - \bar{Y}_{F,s}} \tag{14}$$

This correlation, derived by Nafziger and Renksizbulut (1988), is based on the experimental data of Renksizbulut (1981) and Downing (1960). Because significant liquid heating will reduce the surface temperature, thereby reducing the surface fuel mass fraction and consequently the mass transfer number, the correction for the effects of liquid phase heating is already implicit in the calculation of $B_M$.

Attention is now shifted from the overall characteristics of heat mass and momentum transport, in order to make a more detailed examination of the transport phenomena at the surface of and within the droplet. Shown in Fig. 6 is the transient development in surface velocity gradients. It is interesting to note that at all times the $\partial v_\theta/\partial r$ term is the largest of the gradients, and barring extreme liquid motion it will dominate the surface shear stress.

The magnitudes of the surface tangential velocity and sur-

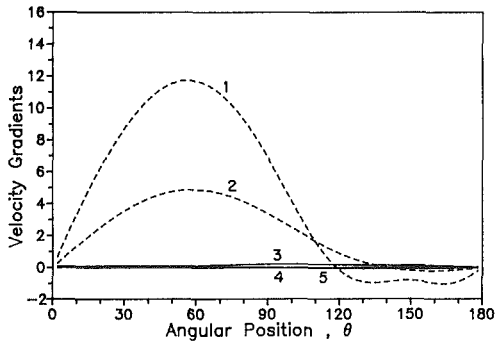


Fig. 6 Surface velocity gradients; (1) $\partial v_\theta/\partial r$ at $t=2000$; (2) $\partial v_\theta/\partial r$ at $t=11{,}000$; (3) $\partial v_r/\partial r$ at $t=2000$; (4) $\partial v_r/\partial\theta$ at $t=2000$; (5) $\partial v_\theta/\partial\theta$ at $t=2000$

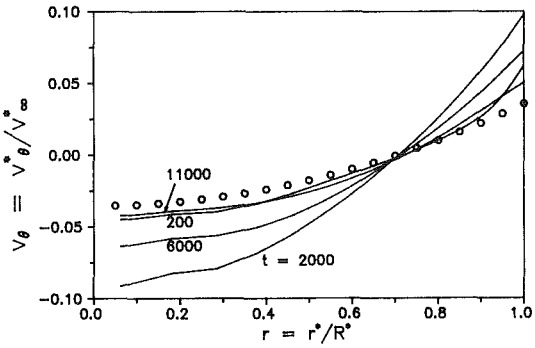


Fig. 9 Tangential liquid velocities along $\theta=90$ deg; ◯ —the Hadamard-Rybczynski solution

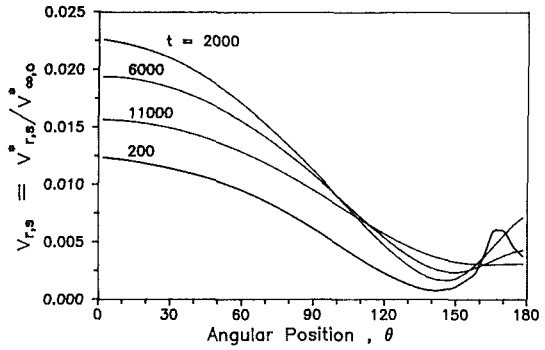


Fig. 7 Surface radial velocity history

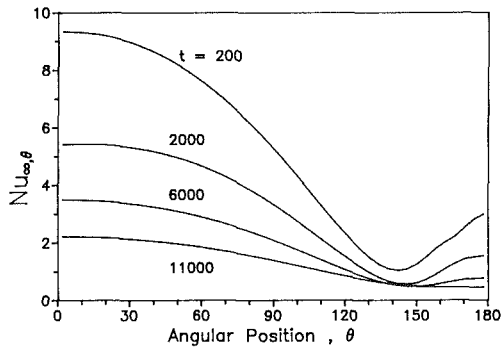


Fig. 10 Local Nusselt number history

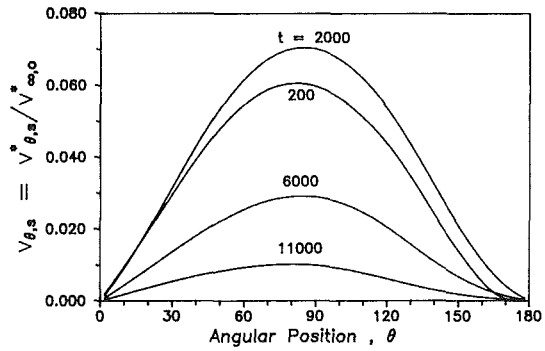


Fig. 8 Surface tangential velocity history

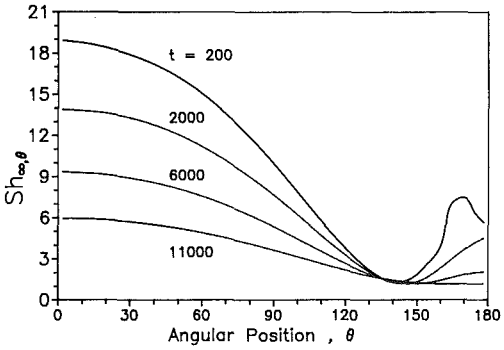


Fig. 11 Local Sherwood number history

face radial gas velocities, scaled with respect to the initial free-stream velocity, are shown in Figs. 7 and 8 for four different times during the transient development. The radial surface velocity peaks early in the lifetime when liquid heating begins to diminish, the surface fuel vapor pressure rises, and convective transport is greatest. As the droplet slows, convection of heat and mass become less effective and vaporization is reduced. The maximum and minimum radial surface velocities occur at the front stagnation point and at the point of flow separation, respectively, at all times. The tangential surface velocity peaks at a maximum of about 7 percent of the free-stream occurring at about $\theta=80$ deg, just aft of the region of maximum aerodynamic shear, early in the lifetime. The intensity of the surface motion decays beyond that time as a result of the droplet deceleration, although the azimuthal location of the maxima remains essentially temporally invariant.

The transient evolution of tangential velocities within the droplet along the plane $\theta=90$ deg is shown in Fig. 9. The liquid circulation is established quickly and a rapid rise in liquid velocities througout the droplet is observed. A gradual decline follows, caused by the transient reduction in free-stream Reynolds number. The rapid increase in the liquid phase velocities, peaking before 10 percent of the droplet lifetime has elapsed, reinforces the arguments of Prakash and Sirignano (1978) that the characteristic time to establish liquid phase motion is short and that the liquid motion can be considered quasi-steady. The results show however that the intensity of liquid phase motion does vary considerably during the droplet lifetime and that the transient effect of droplet deceleration produces profound transient variations in liquid phase motion. Also shown in Fig. 9 are the velocities predicted by the Hadamard-Rybczynski solution. Clearly, the liquid flow field is not predicted well by this creeping flow analysis, except at the lower free-stream Reynolds numbers encountered towards the end of the droplet lifetime. It would appear that the liquid phase flow model proposed by Prakash and Sirignano (1978), consisting of a core region of Hills Spherical vortex and a thin laminar boundary layer at the gas/liquid interface, is more in line with the observed high liquid Reynolds number flow but direct comparison is difficult because predicted liquid velocities are not presented in their work.

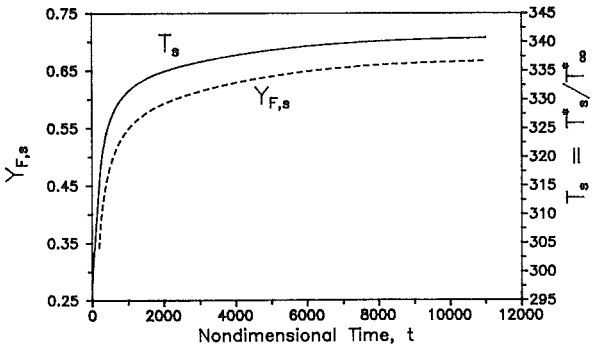


Fig. 12 Average surface temperature and fuel mass fraction histories;—$T_S$; - - - $Y_{F,S}$

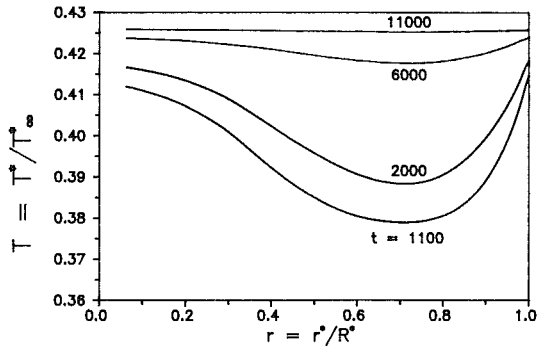


Fig. 13 Liquid temperatures along $\theta = 90$ deg

The transient evolution of the local Nusselt and Sherwood numbers are shown in Figs. 10 and 11, respectively. The reduction in convective heat and mass transport arising from the transient decay in free-stream Reynolds number is seen directly in the reduction in the Nusselt and Sherwood numbers at the stagnation point and in the wake region. As expected, the minima occur very near the point of flow separation and proceed rearward with time. From the results of the present analysis it can be shown that ignoring contributions from the wake region, defined for convenience as $\theta \geq 120$ deg, results in errors in the prediction of the average Nusselt number of 6.4, 6.1, 7.0, and 9.3 percent for $t = 200$, 2000, 6000, and 11,000, respectively. This is in agreement with the postulated error of Prakash and Sirignano (1980) of about 15 percent in boundary layer types of analyses.

The transient histories of the average surface temperature and fuel mass fraction are shown in Fig. 12. It is worth noting that angular variations in the surface temperature were most pronounced early in the droplet lifetime. For example the range in surface temperatures at $t = 200$ was between 313K and 332K about a surface area weighted average of 315K. The strong sensitivity of vapor pressure to temperature is responsible for the unusual bump in the Sh variation observed in Fig. 12 at $t = 200$ in the wake region.

As discussed previously and shown in Fig. 3, liquid phase heating absorbs a significant fraction of the energy available at the droplet surface for about half the droplet lifetime. This result is expected because, as many researchers have indicated, the diffusion of heat in the liquid phase is the slowest transport process inherent to the problem. The qualitative nature of liquid heating can be best understood by examination of the liquid phase temperature contours shown in Fig. 2 and the liquid temperature profiles along the plane ($\theta = 90$ deg) shown in Fig. 13. It is clear that the liquid temperature does not remain spatially invariant and, in spite of the intense liquid motion, the so-called rapid mixing model of liquid phase

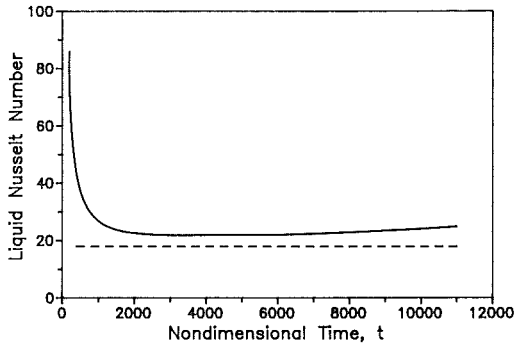


Fig. 14 Liquid Nusselt number history;—fully numerical solution; - - - asymptotic value of Johns and Beckmann (1966)

heating is not applicable. The self-similar nature of the temperature profiles as shown in Fig. 13 suggests that the liquid temperature field quickly reaches an asymptotic profile and that the liquid heating may be in some sense quasi-steady. Adopting the methodology of Johns and Beckmann (1966) a liquid Nusselt number can be defined based on the difference between the liquid surface and volume average temperatures, viz.,

$$\mathrm{Nu}_l = \frac{1}{\bar{k}_l} \int_0^\pi \frac{2k_l}{(\bar{T}_s - \bar{T}_l)} \frac{\partial T}{\partial r}\bigg)_{s,\theta,l} \sin\theta \, d\theta \qquad (15)$$

Figure 14 shows the transient evolution $\mathrm{Nu}_l$. A rapid initial decrease, associated with the establishment of the liquid phase "quasi-steady" temperature field, followed by a nearly constant $\mathrm{Nu}_l$ of about 22 for the duration of the liquid heating period, is observed. It appears that the concept of an asymptotic Nusselt number of Johns and Beckmann is applicable in this case. For the problem investigation the liquid Peclet numbers defined analogously to Johns and Beckmann, viz.,

$$\mathrm{Pe}_l = \frac{\mathrm{Re}_{\infty,0}\mathrm{Pr}_\infty}{4}\left(\frac{1}{1+\mu_l/\mu_\infty}\right) (\rho_l^*/\rho_\infty^*)\,(c_{p,l}^*/c_{p,\infty}^*)\,(k_\infty^*/k_l^*) \qquad (16)$$

are of order 1000, hence their results would predict an asymptotic $\mathrm{Nu}_l$ of 17.9, which is the Kronig and Brink (1950) limit. The discrepancy is expected since the Johns–Beckmann data were based on an assumed velocity field corresponding to the Hadamard–Rybczynski solution, shown earlier not to be representative of the actual situation during most of the droplet lifetime, nor does their solution include the effects of variable properties. Because the ratios of specific heat, thermal conductivity, viscosity, and density for typical liquid hydrocarbons and air at 1 atm pressure will be of order 1, 1, 10, and 1000, respectively, the liquid Peclet number as defined by equation (16) will generally be of order 1000 for droplets initially in the intermediate Reynolds numbers range. It is hypothesized that the observed constant liquid Nusselt number behavior is typical for fuel droplets evaporating in air at intermediate Reynolds numbers and low ambient pressures. Figure 14 does not display any of the oscillations found by Johns–Beckmann attributable to the initial circulations of the liquid phase, but this is not unexpected since the boundary conditions for the present problem result in an increasing surface temperature whereas Johns–Beckmann assumed a constant surface temperature. In previous work by Renksizbulut and Haywood (1986, 1988), studying heptane droplets evaporating in their own vapor, a situation in which the surface temperature remains at the boiling point at all times, such oscillations were observed.

## 4 Conclusions

The transient drag coefficient and Nusselt and Sherwood number histories computed by the complete numerical model

are well predicted by the quasi-steady correlations of Renksizbulut and Yuen (1983a, 1983b) and Renksizbulut and Nafziger (1988). It is concluded therefore that transient effects in the gas phase, the recession of the gas/liquid interface, and second-order drag effects are unimportant at lower pressures ($p \leq 10$ atm). The deceleration of the droplet under the influence of its own drag has been shown to be an important transient effect and for droplets with initial Reynolds numbers of order 100, reductions in the Reynolds number of an order of magnitude can be expected over the droplet lifetime, during which about 80 percent of the original mass is vaporized.

Although the liquid phase motion has been shown to adjust very quickly in response to the shear imparted by the gas phase, the transient decline in the free-stream Reynolds number results in a slow transient decline in the liquid phase motion and in this sense the liquid motion must be considered unsteady.

Liquid phase heating has also been shown to display unsteady behavior. The transient rise in the droplet average and surface temperatures persists for a significant portion of the droplet lifetime. In spite of this unsteadiness, the nature of the liquid phase heating, as characterized by the liquid Nusselt number, has been shown to remain relatively constant. Although the observed asymptotic liquid Nusselt number did not agree with the Kronig and Brink limit, the concept of a rapid approach to a limiting liquid phase Nusselt number appears conceptually correct, and we expect this may generally be true for typical hydrocarbons evaporating in air at low ambient pressures. Departure of the observed liquid Nusselt number from the exact Kronig and Brink limit is due to the considerably higher Reynolds number flow in the present situation as well as variable property effects.

## References


Cliffe, K. A., and Lever, D. A., 1984, "Isothermal Flow Past a Blowing Sphere," TP.1042, Theoretical Physics Division, AERE, Harwell, Oxfordshire, United Kingdom.

Clift, R., Grace, J. R., and Weber, M. E., 1978, *Bubbles, Drops and Particles*, Academic Press, New York.

Downing, C. G., 1960, "The Effect of Mass Transfer on Heat Transfer in the Evaporation of Drops of Pure Liquids," Ph.D. Thesis, University of Wisconsin, WI.

Dwyer, H. A., and Sanders, B. R., 1984a, "Droplet Dynamics and Vapourization With Pressure as a Parameter," ASME Paper No. 84-WA/HT-20.

Dwyer, H. A., and Sanders, B. R., 1984b, "Detailed Computation of Unsteady Droplet Dynamics," *Twentieth Symp. (Int.) in Combustion*, Ann Arbor, MI, pp. 1743-1749.

Faeth, G. M., and 1983, "Evaporation and Combustion of Sprays," *Proc. Energy Combust. Sci.*, Vol. 9, pp. 1-76.

Haywood, R. J., 1986, "Variable-Property, Blowing and Transient Effects in Convective Droplet Evaporation With Internal Circulation," M.A.Sc. Thesis, University of Waterloo, Ontario, Canada.

Haywood, R. J., and Renksizbulut, M., 1986, "On Variable-Property, Blowing and Transient Effects in Convective Droplet Evaporation With Internal Circulation," *Proceedings of the Eighth International Heat Transfer Conference*, San Francisco, CA.

Johns, L. E., Jr., and Beckmann, R. B., 1966, "Mechanism of Dispersed-Phase Mass Transfer in Viscous, Single-Drop Extraction Systems," *AIChE Journal*, Vol. 12, pp. 10-16.

Kronig, R., and Brink, J. C., 1950, "On the Theory of Extraction From Falling Droplets," *Appl. Sci. Res.*, Vol. A2, p. 142.

LeClair, B. P., Hamielec, A. E., Pruppacher, H. R., and Hall, W. D., 1972, "A Theoretical and Experimental Study of the Internal Circulation in Water Drops Falling at Terminal Velocity in Air," *Journal of the Atmospheric Sciences*, Vol. 29, pp. 728-740.

Law, C. K., 1976, "Unsteady Droplet Combustion With Droplet Heating," *Combust. Flame*, Vol. 26, pp. 17-22.

Law, C. K., and Sirignano, W. A., 1977, "Unsteady Droplet Combustion With Droplet Heating—II: Conduction Limit," *Combust. Flame*, Vol. 28, pp. 175-186.

Nafziger, R., 1988, "Convective Droplet Transport Phenomena in High-Temperature Air Streams," M.A.Sc. Thesis, University of Waterloo, Ontario, Canada.

Prakash, S., and Sirignano, W. A., 1978, "Liquid Fuel Droplet Heating With Internal Circulation," *Int. J. Heat Mass Transfer*, Vol. 21, pp. 885-895.

Prakash, S., and Sirignano, W. A., 1980, "Theory of Convective Droplet Vaporization With Unsteady Heat Transfer in the Circulating Liquid Phase," *Int. J. Heat Mass Transfer*, Vol. 23, pp. 253-268.

Ranz, W. E., and Marshall, W. R., 1952, "Evaporation From Drops—I and II," *Chemical Engineering Progress*, Vol. 48, No. 3, pp. 141-173.

Renksizbulut, M., 1981, "Energetics and Dynamics of Droplet Evaporation in High Temperature Intermediate Reynolds Number Flows," Ph.D. Thesis, Northwestern University, Evanston, IL.

Renksizbulut, M., and Haywood, R. J., 1988, "Transient Droplet Evaporation With Variable Properties and Internal Circulation at Intermediate Reynolds Numbers," *Int. J. of Multiphase Flow*, Vol. 14, pp. 189-202.

Renksizbulut, M., and Yuen, M. C., 1983a, "Numerical Study of Droplet Evaporation in a High-Temperature Air Stream," ASME JOURNAL OF HEAT TRANSFER, Vol. 105, pp. 389-397.

Renksizbulut, M., and Yuen, M. C., 1983b, "Experimental Study of Droplet Evaporation in a High-Temperature Air Stream," ASME JOURNAL OF HEAT TRANSFER, Vol. 105, pp. 384-388.

Renksizbulut, M., and Nafziger, R., 1988, paper in preparation.

Sirignano, W. A., 1983, "Fuel Droplet Vaporization and Spray Combustion Theory," *Prog. Energy and Combust. Sci.*, Vol. 9, pp. 291-322.

Spalding, D. B., 1953, "Experiments on the Burning and Extinction of Liquid Fuel Spheres," *Fuel*, Vol. 32, pp. 169-185.

Sundararajan, T., and Ayyaswamy, P. S., 1984, "Hydrodynamics and Heat Transfer Associated With Condensation on a Moving Drop: Solutions for Intermediate Reynolds Numbers," *J. Fluid Mech.*, Vol. 149, pp. 33-58.

Yuen, M. C., and Chen, L. W., 1976, "On Drag of Evaporating Liquid Droplets," *Combustion Sci. Tech.*, Vol. 14, pp. 86-91.